Supporting Information

Vilar *et al.* 10.1073/pnas.0712179105

SI Text

Fibril Growth of α-Synculein. For the presented studies on amyloid fibrils of α-syn, wild-type full-length human α-syn and a shorter variant, α-syn (30–110), which comprises residues 30–110 of human α-syn, were used. α-syn (30–110) was constructed, because EPR measurements (1), solid-state NMR (2), limited proteolysis experiments (3), and quenched H/D exchange NMR (Fig. 1) indicated that only residues 30–110 are folded in the fibrils, whereas the N-terminal ≈30 residues are heterogeneous or flexible and the C-terminal ≈40 residues are of a flexible nature. Both α-syn and α-syn (30–110) were purified from *Escherichia coli* by using standard procedures. Amyloid fibrils were grown by incubation at 37°C with slight agitation in Eppendorf tubes coated with a low-retention polymer as suggested by J. Kelly (personal communication). Fig. S2 shows the kinetics of fibril formation of α-syn and α-syn (30–110) monitored by using Thioflavin-T binding accompanied by circular dichroism (CD) spectroscopy and electron microscopy (EM). The thioflavin T (Thio T) binding kinetics of α-syn fibrils (Fig. S2*C*) resembles a kinetic rate similar to previously published observations by different laboratories (4, 5). The kinetics of α-syn (30–110) fibril formation is faster than wild-type α-syn, which is consistent with the observations that there is an inhibitory action of the C-terminal segment of α-syn in amyloid formation (6, 7), and that α-syn (1–87) aggregates faster than wild type (8). CD spectroscopy indicates a transition into a β-sheet structure on incubation for both α-syn and α-syn (30–110), respectively. The end stage of the conformational transition of both α-syn and α-syn (30–110) are fibrils as evidenced by EM (Fig. S2*B* and Fig. S2*C*). In summary, α-syn (30–110) and α-syn appear to have similar aggregation properties.

Solvent-Accessible Side Chains of α-Synuclein Fibrils. To Identify solvent-exposed amino acid side chains located in α-syn fibrils we used a fluorescent method (9), which measures the labeling efficiency of a fluorescence probe to an artificially introduced cysteine in an α-syn mutants (i.e., V26C, A30C, K34C, E35C, V37C, L38C, Y39C, V40C, K45C, V49C, V52C, T54C, V55C, V63C, V66C, G68C, V71C, T72C, V74C, Q79C, E83C, G86C, A89C, A90C, T92C, and in A124C located in the flexible C-terminal segment). These variants form fibrils as measured by EM (data not shown) with similar properties as wild-type α-syn (10). Fig. 2*D* shows the labeling efficiencies of the various Cys variants relative to the A124C variant, which, based on H/D exchange measurements, should be highly flexible. Overall the labeling efficiencies to Cys side chains in the core region are small when compared with the A1234C mutant. This finding suggests a tight packing of the core. Only the side chains of residues 86, 89, and 90 are highly labeled. Furthermore, the Cys side chains of residues 39, 49, 63, 66, 68, 71, 86, 89, 90, and 92 appear to be significantly more solvent accessible to the fluorescence probe, than residues 26, 30, 37, 38, 45, 52, 54, 74, 79, and 83, which show labeling efficiencies similar to wild-type α-syn that has no Cys. (Note: the 6% labeling efficiency of wild-type α-syn is indicated by a red dotted line in Fig. 2*D*.) Similar findings have been documented by recent EPR studies measuring residue-specific solvent accessibility of Cys variants of α-syn (10). Only residues 89–92 appear to be not solvent-exposed in the EPR study (10). The measured solvent expositions of the Cys side chains of residues 39, 49, 66, 68, 86, 89, and 90 are also consistent with the H/D exchange data showing fast exchange of nearby amides (Fig. 2). A possible explanation for the data of residues 86, 89, and 90 might be that the side chains of β-strand 5 are more solvent-accessible than the other β-strands. The finding that the side chain of Tyr-39 might be partially solvent-accessible is in agreement with the observation by Fink and collaborators (11) that the aromatic ring of Tyr-39 is partially on the surface of the fibrils or in a polar environment. The combination of these data, including the weak alternate pattern of more-and-less solvent exposition of the side chains of residues 37–40, which was also observed in the EPR study (10), suggest that the β-strands 1 and 5 are partially solvent-exposed and that also the loops and, in particular, the loop between β3 and β4, are partially solvent-exposed. The side chains of the residues with odd numbering of β-strands 1 and 5 may face thereby the solvent. Because the introduction of a Cys residue might alter the conformation of α-syn in the amyloid fibril, the solvent accessibility study presented must be interpreted with caution and is used here only in combination with other experimental data.

Material and Methods. ***Cloning and protein expression.*** The expression plasmid of α-syn is the gift of M. Goedert (Medical Research Council, Cambridge, UK). The α-syn variants, i.e., α-syn (30–110) comprising residues 30–110 of α-syn, as well the Cys variants V26C, A30C, 34C, E35C, V37C, L38C, Y39C, V40C, K45C, V49C, V52C, T54C, V55C, V63C, V66C, G68C, V71C, T72C, V74C, Q79C, E83C, 86C, A89C, A90C, and T92C and A124C were constructed by using the QuikChange protocol (Strategene). The fidelity of the PCR products was confirmed by automated nucleotide sequencing. The protocol for the production and purification of α-syn and variants thereof was the one described in Der-Sarkissian *et al.* (1). The quality of the protein purification was checked by SDS-gels and in house mass spectrometry.

Circular dichroism spectroscopy (CD). Wild-type α-syn and α-syn (30–110), at a concentration of 10 mg/ml in PBS pH 7.4, 0.01% sodium azide, were prepared and incubated at 37°C with slight agitation. This is the standard condition used to grow α-syn fibrils for all experiments studied. Spectra were acquired by using an instrument of BioLogic MOS-450 (Molecular Kinetics). All measurements were done at 23°C. Spectra were generally recorded over the wavelength range of 196–260 nm.

Thioflavin T (Thio-T) binding. Wild-type α-syn and α-syn (30–110), at a concentration of 10 mg/ml in PBS pH 7.4 and 0.01% sodium azide, were prepared and incubated at 37°C with slight agitation. Each day, a 10-μl aliquot was diluted with 490 μl of PBS, pH 7.4. The solution was mixed with 10 μl of 1 mM Thio-T prepared in the same buffer. Fluorescence was measured immediately after addition of Thio-T. The measurements were made by using a spectrofluorimeter (Photon Technology International) with excitation at 450 nm and emission at 482 nm. A rectangular 10-mm quartz microcuvette was used. Three independent experiments were performed for each sample.

Electron microscopy (EM). For negative stain transmission electron microscopy samples were prepared at the completion of fibril assembly, 5 ml of each sample at a concentration ≈50 mM were adsorbed onto a glow-discharged, carbon-coated Formvar grid (Electron Microscopy Sciences), incubated for 5 min, washed with distilled water, and then stained with 1% (wt/vol) aqueous uranyl formate solution. EM analysis was performed by using a JEOL JEM-100CXII transmission electron microscope. Images were recorded digitally by using the SIS Megaview III imaging system. For cryo and cryo-negative stain transmission electron microscopy amyloid fibrils of wild-type α-syn and α-syn (30–110)

were applied to EM grids coated with holey carbon film (Quantifoil Micro Tools GmbH). The grids were blotted and quick-frozen by plunging into liquid ethane to obtain unstained vitrified cryo-electron microscopy specimen (12). Alternatively, for cryo-negative staining EM, the sample was applied to the holey carbon grids and stained by layering on a 100-μl drop of saturated ammonium molybdate, pH 7, for 30 s, before the grid was blotted and vitrified (13). These samples were imaged by using a JEOL JEM-2100F transmission electron microscope, operated at 200 keV and a nominal magnification of 50,000×, under minimum dose procedures on a Tietz 4096 × 4096 pixel CCD camera, or on Kodak ISO-163 films, which were developed in full-strength Kodak D19 developer and digitized by using a Heidelberg Primescan D8200 scanner at 2Å/pixel on the sample level.

Computer image processing. The filaments were manually identified by using the programs "helixboxer" and "boxer" in the software package EMAN (14). All of the following image processing was made in the software package SPIDER (15). For image processing of the straight filament, images of 42 filaments were used for windowing 256 particles of 128 × 128 pixel size, sampling a total length of 6.55 μm. These particle images were centered and vertically aligned, followed by classification by correspondence analysis and hierarchical clustering. Class averages were calculated and iteratively used as new references for multireference alignment of the 256 particle images. After five alignment iterations, class averages had converged, and the particles were again subjected to classification and averaged.

For helical image processing of a twisted filament, 492 particles were windowed from the 195-nm-long filament that is shown in Fig. 5*B Central*. These particles were centered and used for a helical 3D reconstruction, by using the repeat length of 130 nm for a full 360° turn of the filament. The handedness of the 3D reconstruction was not determined. The resolution of the 3D reconstruction was determined at 3.3 nm, using the rmeasure program (16).

H/D exchange. For the quenched H/D-exchange studies, amyloid fibrils of recombinant ^{15}N-labeled α-syn or ^{15}N-labeled α-syn (30–110) were used. The samples were either 2 weeks old or 6 months old. To start the hydrogen exchange, the fibrils were sedimented at 3,600 × *g* for 10 min, washed with PBS, pH 7.4, and resuspended in D_2O. At suitable intervals between 0 h and 30 months, aliquots were sedimented at 24,000 × *g* for 2 min, and frozen in liquid nitrogen to quench hydrogen exchange. For the NMR analysis, the fibrils were dissociated in perdeuterated dimethyl sulfoxide (d_6-DMSO) containing 0.1% deuterated trifluoroacetic acid (d_1-TFA). The amount of residual D_2O was estimated to be ≈3%. Immediately after dissolving the fibrils, a series of 80 2D [^{15}N,^{1}H] correlation spectra were measured for 8 h. To distinguish residues that display fast exchange in the fibrils and residues that have high intrinsic exchange rates in DMSO, which would both result in absent peaks in the [^{15}N,^{1}H] correlation spectrum (17), a second series of 80 2D spectra were measured on addition of 3% H_2O. With the exception of some ^{15}N–^{1}H backbone moieties a complete sequence-specific assignment of the backbone ^{15}N–^{1}H cross-peaks was obtained by using the triple-resonance experiments HNCA (18) and HN(CO-)CANH (19) applied to ^{13}C,^{15}N-labeled α-syn (30–110). Some additional resonances were assigned by measuring the above-mentioned triple resonance experiments with full-length α-syn. The data were analyzed by using the programs PROSA (20) and CARA (http://www.nmr.ch), and a specially written Visual basic program in combination with Microsoft Excel (17).

Side-chain solvent accessibility studies. The Cys variants of α-syn were purified as described above in the presence of 20 mM DTT. For fibril formation the variants were incubated in PBS, pH 7.4, and 20 mM DTT. To prepare the fibrils for the side-chain solvent accessibility studies, the fibrils were sedimented at 24,000 × *g*, the supernatant was removed under nitrogen atmosphere, followed by resuspension of the fibrils in PBS, pH 7.4. This process was repeated twice. To label solvent-accessible Cys residues by chemical cross-linking, 50 mM fibrils were incubated with a 2.5-fold molar excess of Alexa Fluor 488 C5 maleimide (Molecular Probes) for 20 min at room temperature. Next, the fibrils were washed extensively with PBS, pH 7.4, buffer and solubilized with 8 M spectroscopically pure guanidine hydrochloride. For fluorescence spectroscopy, the samples were diluted at least 70-fold into PBS, pH 7.4, buffer. The Alexa Fluor 488 fluorescence (excitation, 493 nm; emission, 516 nm) was measured relative to the fluorescence of tyrosine residues in α-syn. To determine the maximum labeling efficiency (100%), the mutant α-syn(A124C) was used, because residue 124 is located in the solvent-accessible C-terminal segment as evidenced by limited proteolysis (3) and fast H/D exchange (see below). As a control, also the intrinsic labeling efficiency of wild-type α-syn was measured (6%).

Solid-state NMR. Approximately 30 mg of 10-month-old ^{15}N,^{13}C-labeled α-syn (30–110) was washed in H_2O, centrifuged, and partially dried under reduced pressure in a desiccator. The resulting material, which had a gel-like consistency, was packed into ZrO Magic Angle Spinning (MAS) rotors and sealed with two-component epoxy adhesive to prevent further dehydration. Solid-state NMR spectra were recorded on a Varian/Chemagnetics Infinity + 500 spectrometer by using 4-mm double-resonance MAS and 2.5-mm triple-resonance MAS probe heads and on a Bruker AV850 MHz spectrometer by using a triple-resonance 3.2-mm MAS probe head in double-resonance mode.

The 4-mm probe was used for a proton-driven spin diffusion (PDSD) experiments (21) with a mixing time of 250 ms at a spinning rate of 11.25 kHz. A total of 512 t_1 increments with 192 scans per increment and a recycle delay of 2.0 s were acquired by using a States scheme for a total experiment time of 5 days.

The 2.5-mm probe was used for two heteronuclear ^{15}N–^{13}C 2D correlation experiments and a homonuclear ^{13}C–^{13}C correlation experiment. The first of these is a NCA experiment (Fig. S2) by using a APHH CP period (22) to transfer polarization from ^{15}N to ^{13}C (23). Selective transfer from $^{15}N_i$ to the directly bound $^{13}C_i^{\alpha}$ was achieved by using low-amplitude pulses during the CP and placement of the ^{13}C carrier frequency in the C^{α} spectral region (24). The second experiment is a N(CO)CA experiment where the polarization is transferred from ^{15}N to $^{13}C'_{i-1}$ by using a selective APHH CP period followed by a homonuclear DREAM transfer (25, 26) from $^{13}C'_{i-1}$ to ^{13}Czsxα. In both experiments 96 t_1 increments with 480 scans each were acquired. The homonuclear ^{13}C–^{13}C correlation experiment used a DREAM mixing period optimized for recoupling between the aliphatic resonances. A total of 320 t_1 increments with 128 scans per increment were acquired. All three experiments used a States scheme during t_1, a MAS rate of 20.86 kHz, and a recycle delay of 2.0 s.

The 3.2-mm probe was used to acquire a ^{13}C–^{13}C PDSD experiment with a mixing time of 200 ms at a spinning rate of 11.5 kHz (Fig. 4*B*). A total of 2,048 t_1 increments with 96 scans per increment and a recycle delay of 1.5 s were acquired for a total experiment time of 4 days. In addition, a ^{13}C–^{13}C DARR (27) experiment with a mixing time of 250 ms at a spinning rate of 19 kHz with 512 t_1 increments, 512 scans per increment and 1.5-s recycle delay was acquired. The cross-sections of Cε1 50 at 137ppm and Cζ 39 at 154 ppm in Fig. 4 are extracted from this spectrum. Finally a ^{13}C–^{13}C DREAM correlation experiment optimized for transfer in the aliphatic region (Fig. 4*A*) was acquired on the sample at a spinning rate of 22.00 kHz with 2,048 increments in t_1, 64 scans, and 1.5-s recycle delay. All three experiments used a TPPI scheme during t_1 and a 1.5-s recycle delay.

The temperature in all experiments was set to values between 0–10°C to counteract heating effects caused by the rotation. In addition all experiments started with an initial APHH CP period from ^{1}H to ^{13}C or ^{15}N and used ≈100 kHz XiX (28) or TPPM (29) decoupling during t_1 and t_2 and ≈110 kHz CW decoupling during the mixing periods where appropriate. All datasets were processed with nmrPipe (30).

The ^{13}C–^{13}C DREAM spectra together with the ^{13}C–^{13}C PDSD and DARR experiments were used for the identification of spin systems and ^{13}C side-chain assignment. The sequential assignment and the collection of distance restraints were extracted from ^{13}C–^{13}C PDSD and DARR spectra. The assignment was confirmed by the N(CO)CA and NCA correlation spectra by using the CARA program (http://www.nmr.ch).

1. Der-Sarkissian A, Jao CC, Chen J, Langen R (2003) Structural organization of alpha-synuclein fibrils studied by site-directed spin labeling. *J Biol Chem* 278:37530–37535.
2. Heise H, et al. (2005) Molecular-level secondary structure, polymorphism, and dynamics of full-length alpha-synuclein fibrils studied by solid-state NMR *Proc Natl Acad Sci USA* 102:15871–15876.
3. Miake H, Mizusawa H, Iwatsubo T, Hasegawa M (2002) Biochemical characterization of the core structure of alpha-synuclein filaments. *J Biol Chem* 277:19213–19219.
4. Conway KA, et al. (2000) Accelerated oligomerization by Parkinson's disease linked alpha-synuclein mutants. *Ann N Y Acad Sci* 920:42–45.
5. Uversky VN, et al. (2002) Biophysical properties of the synucleins and their propensities to fibrillate: Inhibition of alpha-synuclein assembly by beta- and gamma-synucleins. *J Biol Chem* 277:11970–11978,
6. Kessler JC, Rochet JC, Lansbury PT, Jr (2003) The N-terminal repeat domain of alpha-synuclein inhibits beta-sheet and amyloid fibril formation. *Biochemistry* 42:672–678.
7. Hoyer W, Cherny D, Subramaniam V, Jovin TM (2004) Impact of the acidic C-terminal region comprising amino acids 109–140 on alpha-synuclein aggregation in vitro *Biochemistry* 43:16233–16242.
8. Serpell LC, Berriman J, Jakes R, Goedert M, Crowther RA (2000) Fiber diffraction of synthetic alpha-synuclein filaments shows amyloid-like cross-beta conformation *Proc Natl Acad Sci USA* 97:4897–4902.
9. Ritter C, et al. (2005) Correlation of structural elements and infectivity of the HET-s prion. *Nature* 435:844–848.
10. Chen M, Margittai M, Chen J, Langen R (2007) Investigation of alpha-synuclein fibril structure by site-directed spin labeling. *J Biol Chem* 282:24970–24979.
11. Dusa A, et al. (2006) Characterization of oligomers during alpha-synuclein aggregation using intrinsic tryptophan fluorescence. *Biochemistry* 45:2752–2760.
12. Dubochet J, et al. (1988) Cryo-electron microscopy of vitrified specimens. Q *Rev Biophys* 21:129–228.
13. Adrian M, Dubochet J, Fuller SD, Harris JR (1998) Cryo-negative staining. *Micron* 29:145–160.
14. Ludtke SJ, Baldwin PR, Chiu W (1999) EMAN: Semiautomated software for high-resolution single-particle reconstructions. *J Struct Biol* 128:82–97.
15. Frank J, et al. (1996) SPIDER and WEB: Processing and visualization of images in 3D electron microscopy and related fields. *J Struct Biol* 116:190–199.
16. Sousa D, Grigorieff N (2007) Ab initio resolution measurement for single particle structures. *J Struct Biol* 157:201–210.
17. Luhrs T, et al. (2005) 3D structure of Alzheimer's amyloid-beta(1–42) fibrils. *Proc Natl Acad Sci USA* 102:17342–17347.
18. Grzesiek S, Bax A (1992) Improved 3D triple-resonance NMR techniques applied to a 31 kDa protein. *J Magn Reson* 96:432–440.
19. Bracken C, Palmer AG, III, Cavanagh J (1997) (H)N(COCA)NH and HN(COCA)NH experiments for 1H–15N backbone assignments in 13C/15N-labeled proteins. *J Biomol NMR* 9, 94–100.
20. Guntert P, Dotsch V, Wider G, Wuthrich K (1992) Processing of multi-dimensional NMR data with the new software PROSA. *J Biomol NMR* 2:619–629.
21. Suter D, Ernst RR (1985) Spin diffusion in resolved solid-state NMR spectra. *Phys. Rev B* 32:5608–5627.
22. Hediger S, Meier BH, Ernst RR (1995) Rotor-synchronized amplitude-modulated nuclear magnetic resonance spin-lock sequences for improved cross polarization under fast magic angle sample spinning. *J Chem Phys* 102:4000–4011.
23. Baldus M, Geurts DG, Hediger S, Meier BH (1996) Efficient 15N–13C Polarization Transfer by Adiabatic-Passage Hartmann-Hahn Cross Polarization. *J Magn Reson* 118:140–144.
24. Baldus M, Geurts DG, Meier BH (1998) Broadband dipolar recoupling in rotating solids: a numerical comparison of some pulse schemes *Solid State Nucl Magn Reson* 11, 157–168.
25. Verel R, van Beek JD, Meier BH (1999) INADEQUATE-CR experiments in the solid state. *J Magn Reson* 140:300–303.
26. Verel R, Ernst M, Meier BH (2001) Adiabatic dipolar recoupling in solid-state NMR: the DREAM scheme. *J Magn Reson* 150:81–99.
27. Takegoshi K, Yano T, Takeda K, Terao T (2001) Indirect high-resolution observation of 14N NMR in rotating solids. *J Am Chem Soc* 123:10786–10787.
28. Detken A, et al. (2001) Methods for sequential resonance assignment in solid, uniformly 13C, 15N labelled peptides: quantification and application to antamanide. *J Biomol NMR* 20:203–221.
29. Bennett AE, Rienstra CM, Auger M, Lakshmi KV, Griffin RG (1995) Heteronuclear decoupling in rotating solids *J Chem Phys* 103:6951–6958.
30. Delaglio F, et al. (1995) NMRPipe: A multidimensional spectral processing system based on UNIX pipes. *J Biomol NMR* 6:277–293.
31. Lashuel HA, Hartley D, Petre BM, Walz T, Lansbury PT, Jr (2002) Neurodegenerative disease: amyloid pores from pathogenic mutations. *Nature* 418:291.
32. Garnier J, Gibrat JF, Robson B (1996) GOR method for predicting protein secondary structure from amino acid sequence. *Methods Enzymol* 266:540–543.
33. Pawar AP, et al. (2005) Prediction of ''aggregation-prone'' and ''aggregation-susceptible'' regions in proteins associated with neurodegenerative diseases *J Mol Biol* 350:379–392.

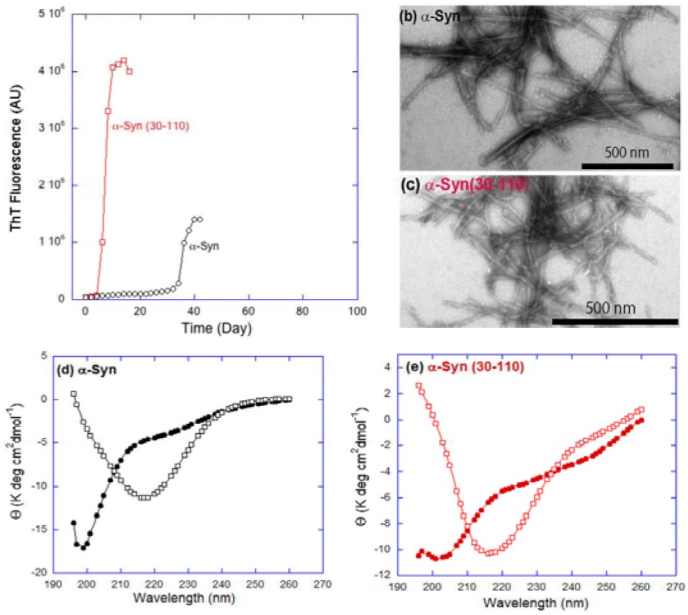

Fig. S1. Aggregation of α-syn and α-syn (30–110). (*a*) Thio T measurement versus time for α-syn (black) and α-syn (30–110) (red) as indicated. The increase of the Thio T is indicative of amyloid formation. For 16 days, 1 mM α-syn and α-syn (30–110) samples were incubated in PBS, pH 7.4, at 37°C under slight agitation. Aliquots thereof were measured by mixing 8–10 μl of sample with 1 ml of 50 mM glycine·NaOH buffer that contained 10 mM ThioT. The ThioT-fluorescence was detected by using an excitation wavelength of 442 nm and an emission wavelength of 485 nm. EM of 16-day-old α-syn (*b*) and α-syn (30–110) (*c*) samples incubated as described in *a*. The EMs show amyloid fibrils for both α-syn and α-syn (30–110). α-syn (30–110) has occasionally also ring-like structures as shown in the middle of *c* (31). (*d* and *e*) CD spectra of α-syn and α-syn (30–110) at day 0 and 16, respectively. The samples were incubated as described in *a*. The comparison between the CD spectra at day 0 and day 16 show nicely the transition into β-sheet structure for both α-syn and α-syn (30–110).

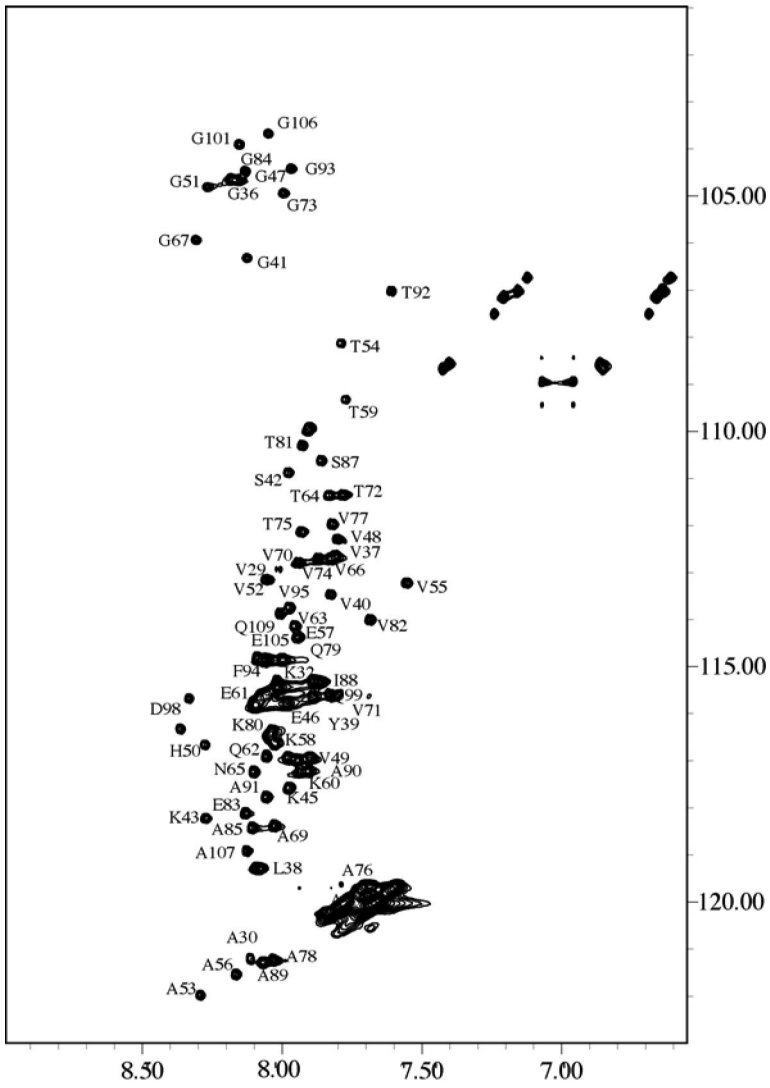

Fig. S2. Peak assignment of [^{15}N,^{1}H]-HMQC-spectrum of ^{15}N-labeled α-syn (30–110) solubilized in d_6-DMSO containing 0.1% d_1-TFA.

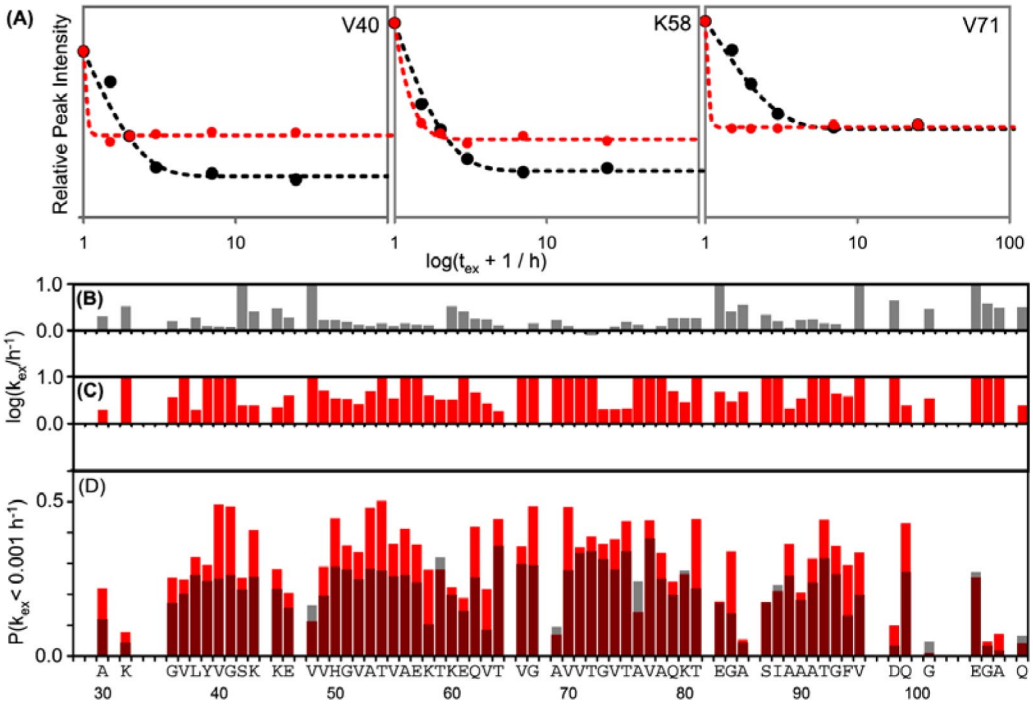

Fig. S3. Detailed H/D exchange analysis of α-syn (30–110) fibrils. The H/D exchange data of 6-month-old α-syn (30–110) fibrils are shown in red. The H/D exchange data of 2-week-old α-syn (30–110) fibrils are shown in black (*A*), gray (*B*), or dark red (*D*). (*A*) H/D exchange curves for several amide moieties as indicated. The peak volumes versus logarithm of the exchange time are shown as spheres. Smooth dotted lines represent a superposition of two monoexponential fits of the raw data. For most residues a biphasic exchange is observed including a slow decay ($\approx$1–10 h) and a very slow decay ($>$ 1,000 h) and the relative population of the exchange changes over time. (*B*) Residue-resolved plot of the H/D exchange rates versus the slow-exchanging population in 2-week-old α-syn (30–110) fibrils. (*C*) Residue-resolved plot of the H/D exchange rates of the slow-exchanging population in 6-month-old α-syn (30–110) fibrils. (*D*) Superposition of the two plots of the fraction of each amide moiety that undergoes H/D exchange very slowly at rates $<$0.001 h^{-1} in 2-week-old (gray) and 6-month-old (red) α-syn (30–110) fibrils. The superposition changes colors, so that red on top of the bars is indicative of a time-dependent increase in protection of the very slowly exchanging conformational species, whereas gray bars indicate a decrease in this species. The amide moieties for which H/D exchange data were obtained are labeled with single-letter amino acid code.

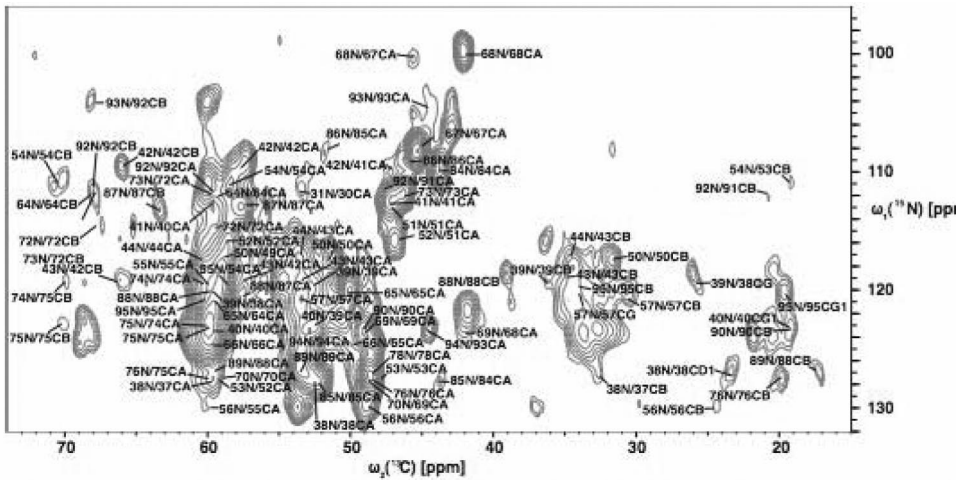

Fig. S4. Solid-state NMR NCA spectrum of α-syn (30–110) fibrils for the sequential assignment. The sequential assignment was obtained by analysis of the ^{13}C–^{13}C proton-driven spin diffusion (PDSD) spectra and the DREAM spectra and confirmed by the sequential backbone spectra from the experiments NCA and N(CO)CA.

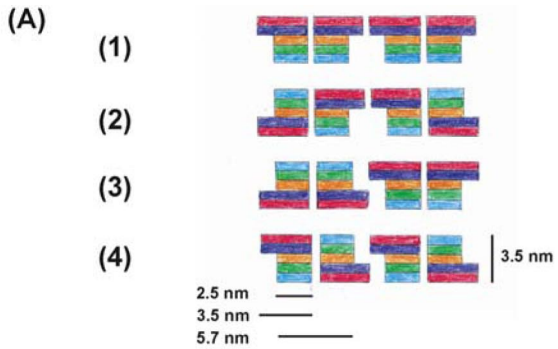

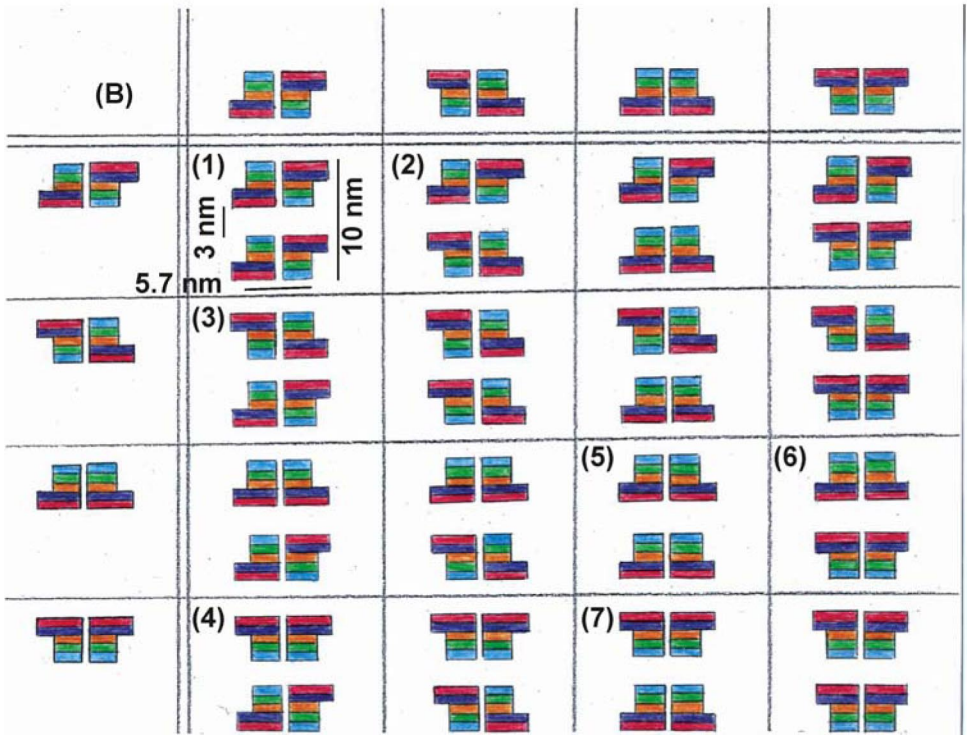

Fig. S5. Possible protofilament packing of straight (*A*) and twisted (*B*) α-syn fibrils. A protofilament is represented by a 2D drawing of the five β-strands of the proposed α-syn fold. The β-strands are color coded in accordance to Figs. 3 and 5. Assuming identical structures between protofiaments, all protofilament packing possibilities are shown. This results in four packing possibilities of 2*2 protofilaments for straight fibrils (*A*) and correspondingly 16 possibilities for twisted fibrils (*B*). Of the four packing possibilities for straight fibrils number 4 is proposed to be the most likely arrangement because it is the only one for which all protofilaments have an unidirectional orientation. This packing is shown in Fig. 5 by a 3D drawing. Of the 16 packing possibilities for twisted fibrils shown in *B* several are degenerate. The remaining seven possible arrangements labeled accordingly can be reduced further in number by a comparison of their predicted electron density with the cryo-EMs shown in Fig. 4. At the widest belly with a measure of 10 nm, the individual protofilaments separated by 3 nm have a size of 3.5 nm. Within this 3.5 nm, the electron density is slightly larger at the edges of the protofilament than in the middle. Such an electron density distribution can be generated only by the packing 1 and 2 labeled. Of the two the packing number 1 is proposed to be the most likely arrangement because in packing 1 all protofilaments have a unidirectional orientation. This packing is shown in Fig. 5 by a 3D drawing.

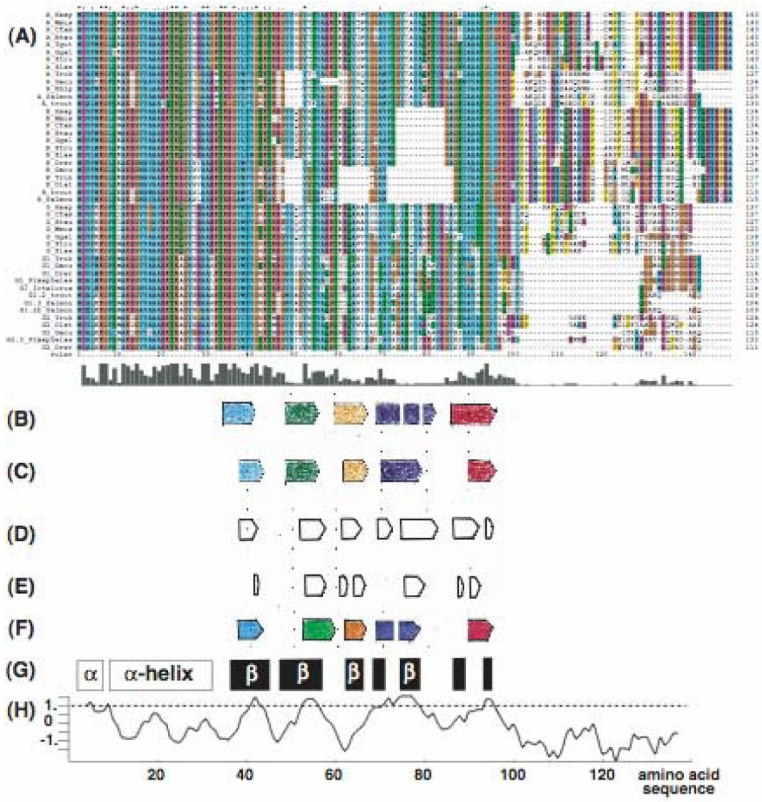

Fig. S6. Primary versus secondary structure of α-syn fibrils. (*A*) Protein sequence alignment of α-, β-, and γ-synuclein from different species abbreviated as follows: Hsap, *Homo sapiens*; Mmus *mus musculus*; Cfam, *Canis famillaris*; Btau, *Bos taurus*; Tgut, *Taeniopygia guttata*; Ggal, *Gallus gallus*; Xtro, *Xenupus tropicalis*; Xlae, *Xenopus laevis*; Trub, *Takifugu rubripes*; Gacu, *Gasterosteus aculeatus*; Hhip, *Hippoglossus hippoglossus*; Olat, *Oryzias latipes*; Drer, *Danio rerio*; Pimephelas, *Pimpephelas promelas*; and Ictalurus, *Ictalurus punctatus*. Identical amino acids conserved between the sequences are color-labeled. The percentage of conservation is represented as a bar diagram below the alignment. (*B* and *C*) The β-strands of the slow-exchanging and the very-slow-exchanging species identified by H/D exchange are indicated along the core sequence of α-syn. (*D* and *E*) The β-strands of the two conformations identified by solid-state NMR by the Baldus group are indicated (2). (*F*) The β-strands of α-syn (30–110) fibrils identified by solid-state NMR. (*G*) β-sheet secondary structure prediction of α-syn by using the algorithm by GOR4 (32). A similar analysis has been presented by Zibaee *et al.* (32). (*H*) Prediction of the aggregation propensity of α-syn by using the algorithm by Vendruscolo (33).